

## Chapter 4: Turbulence at Small Scales

### Part 6: 1D Spatial and Time Series Spectra

We have already noted the following:

1. Most often spectra are obtained from single point time series measurements and transformed to 1D spatial spectra via Taylor's frozen turbulence hypothesis; or in some cases 1D spatial measurements along a line.
2. In either case, the relations between 1D and 3D spectra have shown that the Kolmogorov hypotheses are valid not only for 3D spectra as originally hypothesized, but also for their 1D counterpart.

Herein, we review several techniques for obtaining 1D spectra:

1. Temporal using autocorrelation  $f(t)$  (or convolution integral) and Taylor hypotheses.
2. Spatial using symmetric autocorrelation  $f(r)$  and homogeneous isotropic turbulence assumptions.
3. Spatial using asymmetric autocorrelation  $f(r)$  and nonhomogeneous non-isotropic assumptions.
4. Power Spectral Density (PSD) approach, which is equivalent to technique 1.

Prior to reviewing the techniques for obtaining 1D spectra, power law and model spectrums are discussed, as these will be used in analyzing the 1D spectra and their 3D counterparts using Kolmogorov scaling. Subsequently in Part 7, the 1D and 3D spectra will be further analyzed using alternate scaling such as compensated spectra, etc.

## Power-law spectra

Chapter 4 Parts 0 and 4 already introduced Kolmogorov hypotheses and resulting spectra based on dimensional analysis and its relationship to power law spectra. In the inertial subrange, the power law spectra are of the form

$$E_{11}(\kappa_1) = C_1 A \kappa_1^{-p} \quad (1)$$

Where  $C_1$  is a constant and  $A$  is a normalization factor, e.g.,  $A = \overline{u_1^2} L_{11}^{1-p}$ , i.e., same units as  $\varepsilon^{2/3}$ . If  $E_{11}(\kappa_1)$  is given by (1), then using  $E(k) = f(E_{11}(\kappa_1))$  derived in Part 5, it follows that.

$$E(\kappa) = C A \kappa^{-p}$$

Where  $C = \frac{1}{2} p(2 + p) C_1$ .

Proof in Appendix A.1

Similarly, for  $E_{22}$

$$E_{22}(\kappa) = C_1' A \kappa^{-p}$$

Where  $C_1' = \frac{1}{2} (1 + p) C_1$ .

Proof in Appendix A.2

Thus, the power-law exponent  $p$  is the same for the three spectra and the constants  $C, C_1, C_1'$  are related.

Recall, in the inertial subrange based on dimensional analysis

$$E(\kappa) = C\varepsilon^{2/3}\kappa^{-5/3}$$

Where  $C \sim 1.5$  (from experiments).

Therefore, for  $E_{11}$  and  $E_{22}$

$$E_{11}(\kappa_1) = C_1\varepsilon^{2/3}\kappa_1^{-5/3} \quad \boxed{C_1 = \frac{18}{55}C = 0.49}$$

$$E_{22}(\kappa_1) = C_1'\varepsilon^{2/3}\kappa_1^{-5/3} \quad \boxed{C_1' = \frac{4}{3}C_1 = \frac{24}{55}C = 0.65}$$

### A model spectrum

An analytical model spectrum is used for the evaluation of the Kolmogorov hypotheses and the experimentally (or numerically) obtained spectrums:

$$E(\kappa) = C\varepsilon^{2/3}\kappa^{-5/3}f_L(\kappa L)f_\eta(\kappa\eta) \quad (2)$$

Where  $f_L$  and  $f_\eta$  are specified non-dimensional functions. The function  $f_L$  determines the shape of the energy-containing range,  $f_L \rightarrow 1$  for  $\kappa L \rightarrow \infty$ , i.e., small  $l = 2\pi/\kappa$ . The function  $f_\eta$  determines the shape of the dissipation range,  $f_\eta \rightarrow 1$  for  $\kappa\eta \rightarrow 0$ , i.e., large  $l = 2\pi/\kappa$ .

In the inertial subrange, both  $f_L$  and  $f_\eta \rightarrow 1$  so that the Kolmogorov -5/3 spectrum is obtained with the constant  $C$  recovered.

The specification of  $f_L$  is

$$f_L(\kappa L) = \left( \frac{\kappa L}{[(\kappa L)^2 + c_L]^{\frac{1}{2}}} \right)^{\frac{5}{3} + p_0} \quad (3)$$

$p_0$  is taken to be 2, and  $c_L$  is a positive constant. Clearly,  $f_L \rightarrow 1$  for large  $\kappa L$ , while the exponent  $\frac{5}{3} + p_0$  leads to  $E(\kappa) \propto \kappa^{p_0} = \kappa^2$  for small  $\kappa L$ . Or for  $p_0 = 4$  leads to  $E(\kappa) \propto \kappa^4$  for small  $\kappa L$ .<sup>1</sup>

The specification of  $f_\eta$  is

$$f_\eta(\kappa\eta) = \exp \left\{ -\beta \left\{ [(\kappa\eta)^4 + c_\eta^4]^{1/4} - c_\eta \right\} \right\} \quad (4)$$

Where  $\beta$  and  $c_\eta$  are positive constants. For  $c_\eta = 0$ :  $f_\eta(\kappa\eta) = \exp(-\beta\kappa\eta)$ . In either case, exponential decay is exhibited for large  $\kappa\eta$ .

Since the velocity field  $\underline{u}(\underline{x})$  is infinitely differentiable, for large  $\kappa$ , the energy spectrum decays more rapidly than any power of  $\kappa$ , thus, exponential decay is used, as suggested by Kraichnan. Experiments support exponential decay with  $\beta = 5.2$ . However, the simplified exponential form with  $c_\eta = 0$  departs from unity too rapidly for small  $\kappa\eta$  and the value of  $\beta$  is constrained to be  $\beta = 2.1$ . These deficiencies are remedied by Eq. (4).

---

<sup>1</sup> Chapter 4 Part 5 pg. 7: If  $\mathcal{E}_{ij}(\underline{\kappa})$  is analytic at  $\underline{\kappa}=0$  then  $E(\kappa)$  varies as  $\kappa^4$  for small  $\kappa$  (Pope Ex. 6.26); however, it's also possible that it is non-analytic with  $E(\kappa)$  varying as  $\kappa^2$ . DNS shows both behaviors and some grid turbulence data suggests  $\kappa^2$  behavior.

For specified values of  $k$ ,  $\varepsilon$ , and  $\nu$ , the model spectrum is determined using Eq. (2), (3) and (4) with  $C = 1.5$  and  $\beta = 5.2$ .<sup>2</sup> Alternatively, the non-dimensional model spectrum is uniquely determined by a specified value of  $R_\lambda$ .

$c_L$  and  $c_\eta$  are determined by the requirement that  $E(\kappa)$  and  $2\nu\kappa^2 E(\kappa)$  integrate to  $k$  and  $\varepsilon$ , respectively: at high Re their values are  $c_L \approx 6.78$  and  $c_\eta \approx 0.40$ .

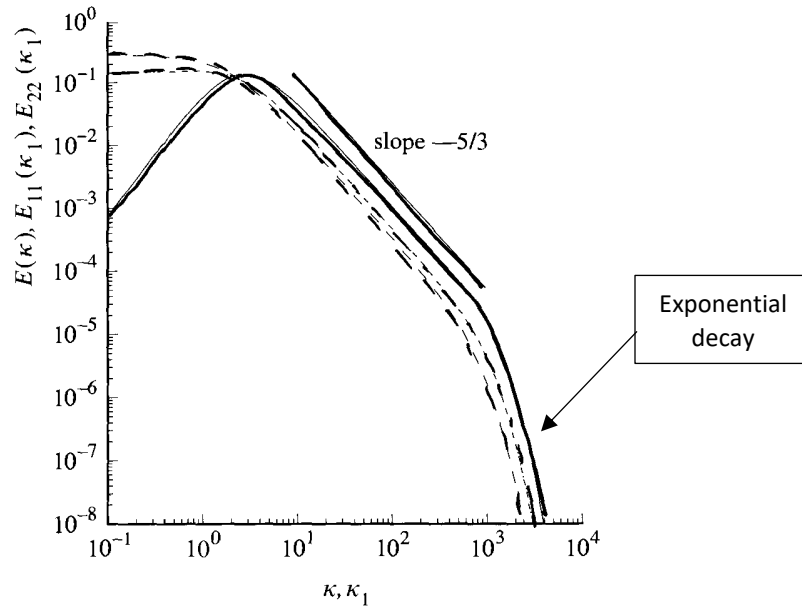


Fig. 6.11. Comparison of spectra in isotropic turbulence at  $R_\lambda = 500$ : solid line,  $E(\kappa)$ ; dashed line,  $E_{11}(\kappa_1)$ ; dot-dashed line,  $E_{22}(\kappa_1)$ . From the model spectrum, Eq. (6.246). (Arbitrary units.)

Fig. 6.11 shows  $E(\kappa)$ ,  $E_{11}(\kappa)$  and  $E_{22}(\kappa)$  at  $R_\lambda = 500$ . In the inertial subrange, all spectra exhibit power-law behavior with  $p = 5/3$ , and their ratio is given by the ratio of  $C$ ,  $C_1$ ,  $C'_1$ .

At low wave number  $E(\kappa) \rightarrow 0$  as  $\kappa^2$ , while one-dimensional spectra are maximum at  $\kappa = 0$ , which shows the effects of aliasing, i.e., the fact that the 1D spectra only contain contributions from  $\kappa > \kappa_1$ .<sup>3</sup> Also, at low wave number

$$E_{11} = 2E_{22}$$

<sup>2</sup> Note that  $k$  and  $\varepsilon$  can be obtained from the macro scales, as per Chapter 4 Part 3

<sup>3</sup> Also see Chapter 4 Part 5 pg. 12.

in accordance with the ratios of integral scales  $L_{11}$  and  $L_{22}$ , i.e.,  $L_{22} = L_{11}/2$ .

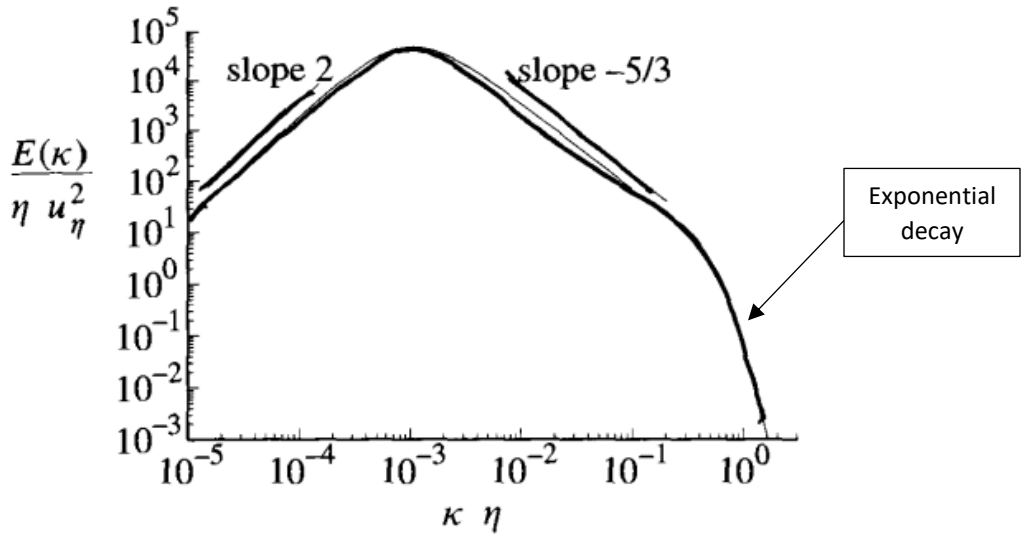
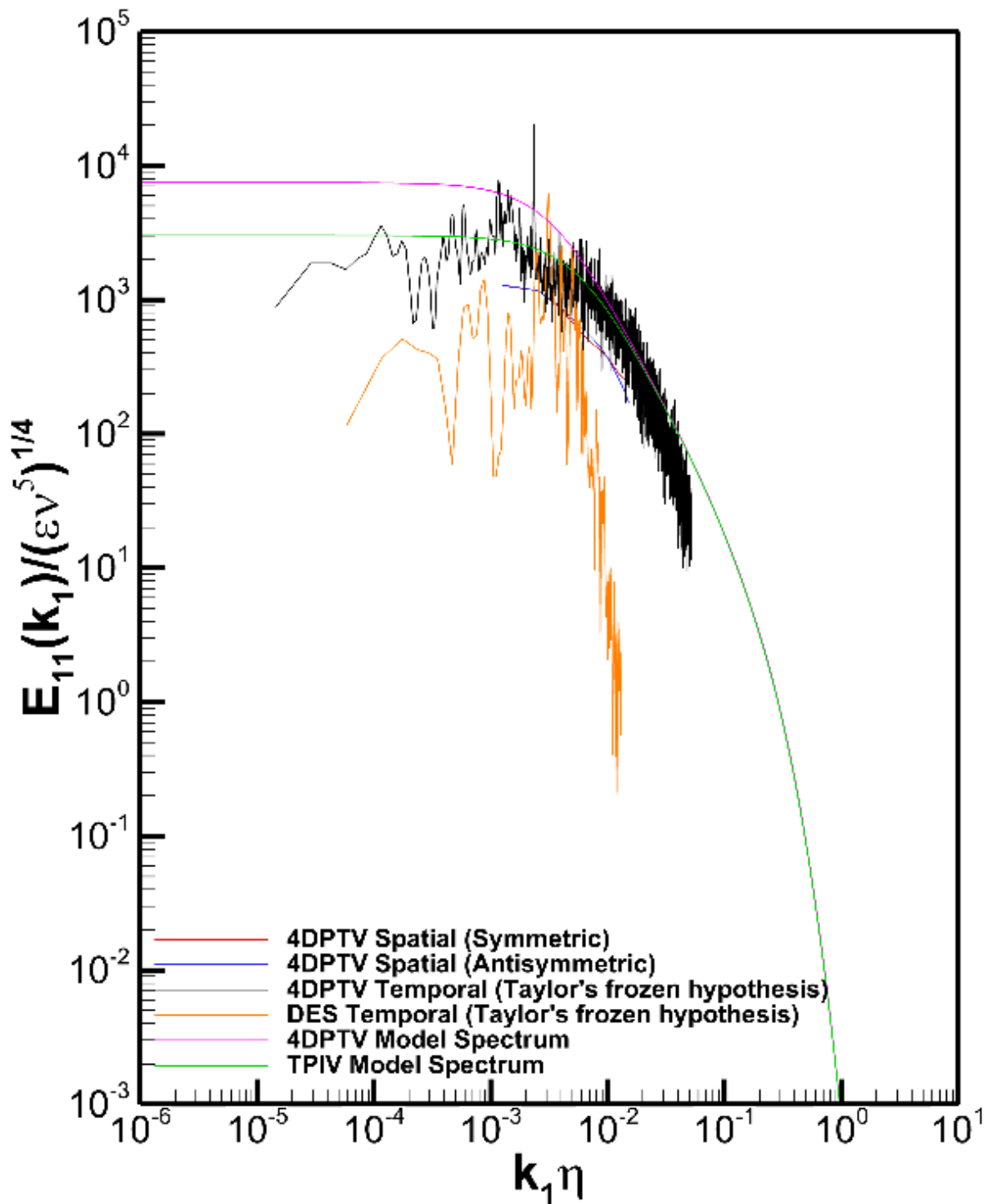


Fig. 6.13. The model spectrum (Eq. (6.246)) for  $R_\lambda = 500$  normalized by the Kolmogorov scales.

The log-log plot of the model spectrum (with Kolmogorov scaling) for  $R_\lambda = 500$  shows the power laws  $E(\kappa) \sim \kappa^2$  at low wave number and  $E(\kappa) \sim \kappa^{-5/3}$  in the inertial subrange and the exponential decay at large  $\kappa$ .



Frederick Stern, Yugo Sanada, Zachary Starman, Shanti Bhushan, Christian Milano, "4DPTV Measurements and DES of the Turbulence Structure and Vortex-Vortex Interaction for 5415 Sonar Dome Vortices," 35th Symposium on Naval Hydrodynamics, Nantes, France, 7 July - 12 July 2024. Turbulence Analysis of SDVP for  $\beta=10^\circ$  at  $x/L=0.12$ . 1D longitudinal velocity spectra shown for Kolmogorov scaling using macro-scale values.

## Techniques for obtaining 1D spectra

### Method 1: Energy Spectrum from spatial autocorrelation $f(r)$ : even

1. Calculate symmetric spatial autocorrelation function.

$$f(r) = \frac{\overline{u(x)u(x+r)}}{\overline{u^2}}$$

2. Obtain 1D energy spectrum from Fourier transform of  $f(r)$

$$E_{11}(\kappa) = \frac{2}{\pi} \overline{u^2} \int_0^{\infty} f(r_1) \cos(\kappa_1 r_1) dr_1$$

3. Calculate the Taylor microscale and integral length scale.

$$\lambda_f = [-2/f''(0)]^{1/2}, \quad \Lambda_f = \frac{1}{2} \int_{-\infty}^{\infty} f(r) dr = \int_0^{\infty} f(r) dr$$

4. Calculate dissipation.

$$\varepsilon = 30\nu \frac{\overline{u^2}}{\lambda_f^2}$$

5. Calculate Kolmogorov scale.

$$\eta = \left( \frac{\nu^3}{\varepsilon} \right)^{1/4}$$

6. Plot  $E_{11}(\kappa_1)/(\varepsilon\nu^5)^{1/4}$  vs  $\kappa_1\eta$

## Method 2: Energy Spectrum from spatial autocorrelation $f(r)$ : odd

1. Calculate the antisymmetric spatial autocorrelation function.

$$f(\pm r) = \frac{\overline{u(x)u(x \pm r)}}{\overline{u^2}}$$

2. Obtain 1D energy spectrum in space from Fourier transform of  $f(r)$

$$E_{11}(\kappa) = \frac{\overline{u^2}}{\pi} \int_{-\infty}^{\infty} f(r_1) \cos(\kappa_1 r_1) d r_1$$

3. Calculate the Taylor microscale and integral length scale.

$$\lambda_f = \frac{\left[ -f'(0) + \left[ \{f'(0)\}^2 - 2f''(0) \right]^{\frac{1}{2}} \right]}{f''(0)}, \quad \Lambda_f = \frac{1}{2} \int_{-\infty}^{\infty} f(r) dr$$

4. Calculate dissipation.

$$\varepsilon = \nu \left( \overline{u_{i,j}u_{i,j}} + \frac{\partial^2 \overline{u_i u_j}}{\partial x_i \partial x_j} \right)$$

5. Calculate Kolmogorov scale.

$$\eta = \left( \frac{\nu^3}{\varepsilon} \right)^{1/4}$$

6. Plot  $E_{11}(\kappa_1)/(\varepsilon\nu^5)^{1/4}$  vs  $\kappa_1\eta$

### Method 3: Energy spectrum from temporal autocorrelation $f(\tau)$

1. Calculate temporal autocorrelation.

$$R_E(\tau) = \frac{\overline{u(t)u(t+\tau)}}{\overline{u^2}}$$

2. Obtain Fourier transform of  $R_E(\tau)$ .

$$\hat{R}_E(2\pi\omega) = 2 \int_0^\infty R_E(\tau) \cos(2\pi\omega\tau) d\tau$$

(Note:  $\omega$ : Frequency [Hz])

3. Calculate the time micro and macro/integral scales.

$$\tau_E = [-2/f''(0)]^{1/2}, \quad T = \int_0^\infty f(\tau) d\tau$$

4. Using Taylor hypothesis, calculate the Taylor microscale, dissipation, and Kolmogorov scale.

$$\lambda_f = \overline{U}\tau_E, \quad \varepsilon = 30\nu \frac{\overline{u^2}}{\lambda_f^2}, \quad \eta = \left(\frac{\nu^3}{\varepsilon}\right)^{1/4}$$

5. Calculate the 1D energy spectrum in time from the Fourier transform of  $R_E(\tau)$ .

$$\hat{E}_{11}(\omega) = 2\overline{u^2}\hat{R}_E(2\pi\omega)$$

6. Calculate the 1D energy spectrum in space from the 1D energy spectrum in time.

$$E_{11}(\kappa_1) = \frac{\overline{U}}{2\pi} \hat{E}_{11}(\omega)$$

7. Plot  $E_{11}(\kappa_1)/(\varepsilon\nu^5)^{1/4}$  vs  $\kappa_1\eta$

### Details Method 3

Taylor's frozen turbulence hypothesis relates time sequence of streamwise velocity data to data distributed along a straight line in the flow direction as if the turbulent velocity field at a given instant in time convects downstream at the local mean velocity, i.e., as if it were frozen.

$$u(x, t + \tau) = u(x - \bar{U}\tau, t) \quad (1)$$

Where  $x - \bar{U}\tau$  represents the upstream point, so that

$$\overline{u(x, t)u(x, t + \tau)} = \overline{u(x, t)u(x - \bar{U}\tau, t)} \quad (2)$$

Combining with  $f(r)$  and  $R_E(\tau)$  definitions

$$f(r) = \frac{\overline{u(x)u(x+r)}}{\overline{u^2(x)}} \quad (3)$$

$$R_E(\tau) = \frac{\overline{u(t)u(t+\tau)}}{\overline{u^2}} \quad (4)$$

Taking  $r = -\bar{U}\tau$  in Eq. (3)

$$f(-\bar{U}\tau) = \frac{\overline{u(x)u(x - \bar{U}\tau)}}{\overline{u^2(x)}}$$

Comparing with Eq. (4) and adding  $t$  dependence to Eq. (3) and  $x$  dependence to Eq. (4)

$$\underbrace{\frac{\overline{u(x, t)u(x, t + \tau)}}{\overline{u^2}}}_{R_E(\tau)} = \underbrace{\frac{\overline{u(x, t)u(x - \bar{U}\tau, t)}}{\overline{u^2}}}_{f(-\bar{U}\tau)} \quad (5)$$

Assuming zero separation ( $x + r = 0$ ,) and zero time-delay ( $t + \tau = 0$ ) and using the symmetry of  $R_E(\tau)$  and  $f(r)$  yields

$$x = \pm r, \quad t = \pm \tau$$

Using these relations in Eqs. (3) and (4), including their  $t$  and  $x$  dependence

$$f(r = x) = \frac{u(x, t)u(0, t)}{\overline{u^2}} \quad (6)$$

$$R_E(\tau = t) = \frac{u(x, t)u(x, 0)}{\overline{u^2}} \quad (7)$$

Comparing the RHS of Eq. (5) and (6), shows that

$$x = \overline{U}\tau \Rightarrow \tau = \frac{x}{\overline{U}} \quad (8)$$

Substituting Eq. (8) into (7) and equating to (6) yields

$$R_E\left(\tau = t = \frac{x}{\overline{U}}\right) = \frac{u\left(x, \frac{x}{\overline{U}}\right)u(x, 0)}{\overline{u^2}} = f(r = x) = \frac{u(x, t)u(0, t)}{\overline{u^2}}$$

$$R_E\left(\frac{x}{\overline{U}}\right) = f(x)$$

Using the definitions of  $E_{11}(k_1)$  and  $\hat{R}_E(\omega')$

$$E_{11}(k_1) = \frac{\overline{u^2}}{\pi} \int_{-\infty}^{\infty} e^{-ik_1 x} f(x) dx$$

$$f(x) = R_E\left(\frac{x}{\overline{U}}\right)$$

$$= \frac{\overline{u^2}}{\pi} \int_{-\infty}^{\infty} e^{-ik_1 x} R_E\left(\frac{x}{\overline{U}}\right) dx$$

$$dx = \overline{U} d\tau$$

$$= \frac{\overline{u^2}}{\pi} \int_{-\infty}^{\infty} e^{-ik_1 \overline{U} \tau} R_E(\tau) \overline{U} d\tau$$

$$\hat{R}_E(\omega') = \int_{-\infty}^{\infty} e^{-i\tau\omega'} R_E(\tau) d\tau$$

$$\begin{aligned} \omega' &= 2\pi\omega \\ \omega &\text{ Hz} \\ \omega' &\text{ rad/s} \end{aligned}$$

From the comparison of the exponentials highlighted in yellow, the following relationship is obtained:

$$k_1 \overline{U} \tau = 2\pi\omega\tau \Rightarrow \omega = k_1 \overline{U} / 2\pi.$$

$$= \frac{\overline{u^2} \overline{U}}{\pi} \int_{-\infty}^{\infty} e^{-i\tau\omega'} R_E(\tau) d\tau = \frac{\overline{u^2} \overline{U}}{\pi} \hat{R}_E(\omega') \quad (9)$$

Recall (Chapter 2)

$$\hat{E}_{11}(\omega) = 2\overline{u^2} \hat{R}_E(2\pi\omega) \quad (10)$$

Combining Eqs. (9) and (10), to obtain a relation between  $\hat{E}_{11}(\omega)$  and  $E_{11}(k_1)$ :

$$E_{11}(k_1) = \frac{\overline{u^2} \overline{U}}{\pi} \frac{\hat{E}_{11}(\omega)}{2\overline{u^2}} = \frac{\overline{U}}{2\pi} \hat{E}_{11}(\omega)$$

Or equivalently

$$\hat{E}_{11}(\omega) = \frac{2\pi}{\overline{U}} E_{11}\left(\frac{2\pi\omega}{\overline{U}}\right)$$

Thus,  $E_{11}(k_1)$  can be determined from measurements of  $\hat{E}_{11}(\omega) = \hat{E}_{11}\left(\frac{k_1 \overline{U}}{2\pi}\right)$ .

Measured time spectra via Taylor hypothesis provide  $E_{11}(k_1)$

Taylor micro-scale

$$\begin{aligned}f(x) &= R_E\left(\tau = \frac{x}{\bar{U}}\right) \\f' &= R_{E,\tau} \frac{d\tau}{dx} = R_E' / \bar{U} \\f'' &= R_E'' / \bar{U}^2 \\ \lambda_f^2 &= -\frac{2}{f''} = -\frac{2\bar{U}^2}{R_E''} = \bar{U}^2 \lambda_t^2\end{aligned}$$

Taylor macro-scale

$$\begin{aligned}\Lambda_f &= \int_0^\infty f(x) dx \\ &= \int_0^\infty R_E(\tau) \bar{U} d\tau \\ \Lambda_f &= \bar{U} \Lambda_t\end{aligned}$$

#### Method 4: Power Spectral Density (PSD) approach

1. Obtain velocity time-series  $u(t)$  either experimentally or DES.
2. Obtain the  $u(t)$  power spectral density  $\text{PSD}^4 = \lim_{T \rightarrow \infty} \frac{1}{2T} |\hat{u}(\omega)|^2 = \hat{E}_{11}(\omega)$  [(m<sup>2</sup>/s<sup>2</sup>)/Hz]. Usually directly via its definition, however, in this case not related to  $R_E(\tau)$  and therefore not able to use proper scaling to obtain the Kolmogorov spectrum. For present purposes can be obtained via the temporal autocorrelation and convolution concept.

$$R_E(\tau) = \frac{\overline{u(t)u(t+\tau)}}{\overline{u^2}} = \frac{\overline{u(t)u(t-\tau)}}{\overline{u^2}}$$

Where the second equality is a consequence of the of the assumption of homogeneous isotropic turbulence. Using the definition of time average:

$$R_E(\tau) = \frac{1}{\overline{u^2}} \frac{1}{2T} \int_{-T}^T u(t)u(t-\tau)dt$$

Taking the limit for  $T \rightarrow \infty$

$$R_E(\tau) = \frac{1}{\overline{u^2}} \lim_{T \rightarrow \infty} \frac{1}{2T} \int_{-T}^T u(t)u(t-\tau)dt$$

Which shows that  $R_E(\tau)$  represents the convolution of the velocity field with itself.

Taking the Fourier transform of  $R_E(\tau)$ :

$$\mathcal{F}\{R_E(\tau)\} = \hat{R}_E(\omega') = \int_{-\infty}^{\infty} \left[ \frac{1}{\overline{u^2}} \lim_{T \rightarrow \infty} \frac{1}{2T} \int_{-T}^T u(t)u(t-\tau)dt \right] e^{-i\omega'\tau} d\tau \quad [s]$$

And using the following substitution of variables:

$$t - \tau = s \Rightarrow \frac{dt}{dt} - \frac{d\tau}{dt} = \frac{ds}{dt} \Rightarrow 1 = \frac{ds}{dt} \Rightarrow ds = dt$$

$$\hat{R}_E(\omega') = \int_{-\infty}^{\infty} \left[ \frac{1}{\overline{u^2}} \lim_{T \rightarrow \infty} \frac{1}{2T} \int_{-T}^T u(t)u(s)dt \right] e^{-i\omega'(t-s)} ds$$

---

<sup>4</sup> Power Spectral Density (PSD) analysis in turbulent velocity examines the distribution of energy across different frequencies, revealing how turbulence energy cascades from large to small scales, and can be used to understand the characteristics of turbulent flows.

Separating the integrals gives:

$$\hat{R}_E(\omega') = \frac{1}{u^2} \lim_{T \rightarrow \infty} \frac{1}{2T} \int_{-T}^T u(t) e^{-i\omega' t} dt \int_{-\infty}^{\infty} u(s) e^{i\omega' s} ds$$

And using the definition of Fourier transform

$$\hat{R}_E(\omega') = \frac{1}{u^2} \lim_{T \rightarrow \infty} \frac{1}{2T} \underbrace{\int_{-T}^T u(t) e^{-i\omega' t} dt}_{\hat{u}(\omega)} \underbrace{\int_{-\infty}^{\infty} u(s) e^{i\omega' s} ds}_{\hat{u}^*(\omega)} \quad \left[ \frac{s^2}{m^2} \frac{1}{s} m^2 = s \right]$$

$$\hat{R}_E(\omega') = \frac{1}{u^2} \lim_{T \rightarrow \infty} \frac{1}{2T} \hat{u}(\omega) \hat{u}^*(\omega) = \frac{1}{u^2} \lim_{T \rightarrow \infty} \frac{1}{2T} |\hat{u}(\omega)|^2$$

$$\hat{E}_{11}(\omega) = 2\overline{u^2} \hat{R}_E(\omega') = \lim_{T \rightarrow \infty} \frac{1}{2T} |\hat{u}(\omega)|^2 \quad [\text{m}^2/\text{s}]$$

3. By definition,  $\hat{R}_E(\omega')$  represents the Fourier transform of  $R_E(\tau)$ . Using the inverse Fourier transform, it is possible to recover  $R_E(\tau)$ :

$$R_E(\tau) = \mathcal{F}^{-1}\{\hat{R}_E(\omega')\} = \frac{1}{2\pi} \int_{-\infty}^{\infty} \hat{R}_E(\omega') e^{i\omega' \tau} d\omega' = \frac{\overline{u(t)u(t+\tau)}}{\overline{u^2}}$$

4. Calculate the time micro and macro/integral scales.

$$\tau_E = [-2/R_E''(0)]^{1/2}, \quad T = \int_0^{\infty} R_E(\tau) d\tau$$

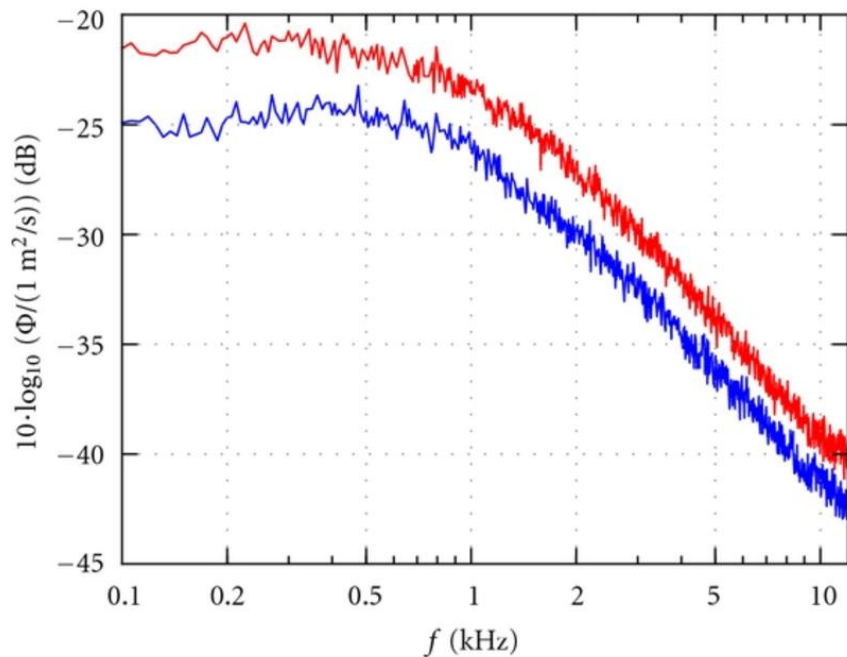
5. Using Taylor hypothesis, calculate the Taylor microscale, dissipation, and Kolmogorov scale.

$$\lambda_f = \overline{U} \tau_E, \quad \varepsilon = 30\nu \frac{\overline{u^2}}{\lambda_f^2}, \quad \eta = \left( \frac{\nu^3}{\varepsilon} \right)^{1/4}$$

6. Calculate the 1D energy spectrum in space from the 1D energy spectrum in time.

$$E_{11}(\kappa_1) = \frac{\overline{U}}{2\pi} \hat{E}_{11}(\omega) \quad [\text{m}^3/\text{s}^2]$$

7. Plot  $E_{11}(\kappa_1)/(\varepsilon\nu^5)^{1/4}$  vs  $\kappa_1\eta$



Power spectral density (re  $1 \text{ (m/s)}^2/\text{Hz}$ ) of the turbulent velocity fluctuations, measured at a nominal flow speed  $U_0=35 \text{ m/s}$  approximately at  $x=-0.154 \text{ m}$ ,  $0.007 \text{ m}$  upstream of the leading edge of the non-porous reference airfoil at mid-span (turbulence grids: (blue —) PPS 12/2, (red —) PPS 14/4).

Convolution

$$h(t) = \int_{-\infty}^{\infty} f_1(t-s) f_2(s) ds \quad f_1(t) \text{ \& } f_2(t) \text{ both via FT}$$

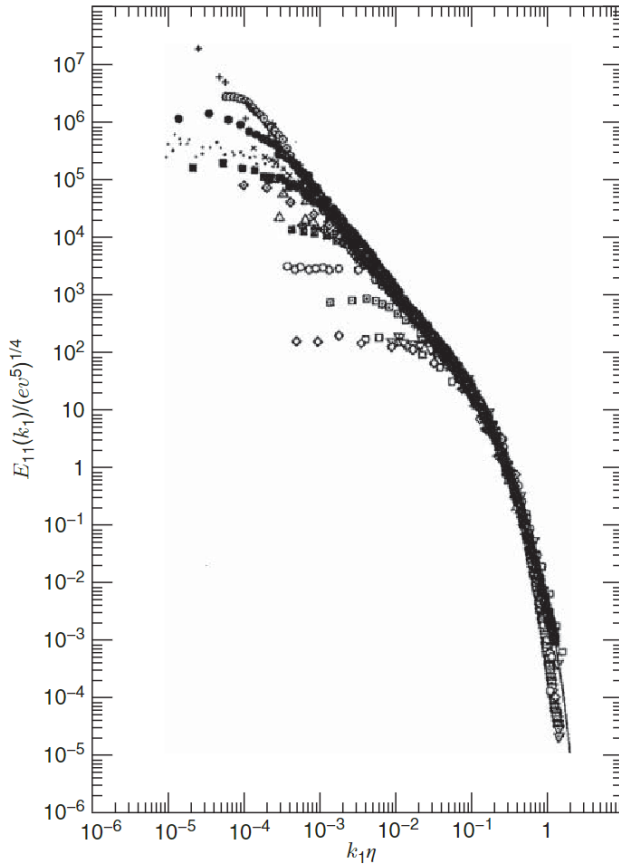
$$F\{h(t)\} = \frac{1}{2\pi} \int_{-\infty}^{\infty} e^{-i\omega t} \int_{-\infty}^{\infty} f_1(t-s) f_2(s) ds dt$$

$$r = t - s \quad = \frac{1}{2\pi} \int_{-\infty}^{\infty} \int_{-\infty}^{\infty} e^{-i\omega(r+s)} f_1(r) f_2(s) ds dr$$

$$= \frac{1}{2\pi} \int_{-\infty}^{\infty} e^{-i\omega r} f_1(r) dr \int_{-\infty}^{\infty} e^{-i\omega s} f_2(s) ds$$

$$= 2\pi F\{f_1(t)\} F\{f_2(t)\}$$

Fourier transform of convolution = product of  $2\pi$  x Fourier transform of the functions.



$$E(k) = (\epsilon v^5)^{1/4} \varphi(k\eta) = \eta u_\eta^2 \varphi(k\eta)$$

$\varphi(k\eta) = \text{Kolmogorov spectrum function.}$

**Figure 4.7** Experimental tests of the  $-5/3$  law [3]. Reprinted with the permission of Cambridge University Press.

Measured scaled spectra clearly show the universal equilibrium range and inertial subrange Kolmogorov  $-5/3$  spectrum, which extends over several decades of wave number. The extent of the inertial subrange increases with  $Re_\lambda$ . Data show  $C_1 \sim .5$  such that  $C \sim 1.4$ . Recent estimates  $Re_\lambda = 1000, C = 1.58$ .

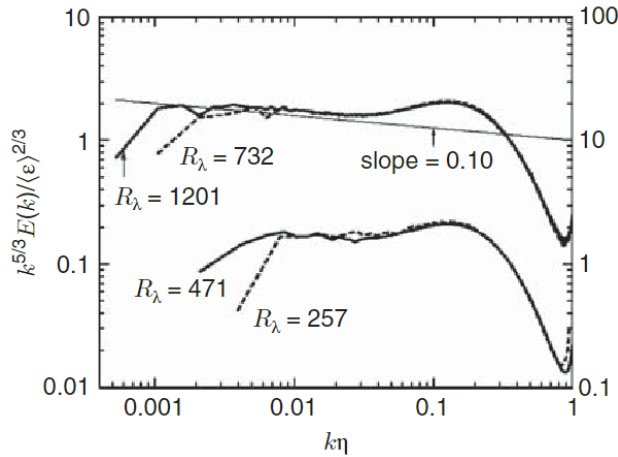


**Figure 4.8** Compensated energy spectrum as given in [21]. With increasing  $R_\lambda$ , the simulations used  $512^3$ ,  $1024^3$ ,  $2048^3$ , and  $4096^3$  meshes. Scales on the left and right are for the upper and lower curves, respectively. Reproduced from *Physics of Fluids*, Vol. 15, pp. L21–L24, 2003, with the permission of AIP Publishing.

Compensated spectrum  $E(k)/\epsilon^{2/3}k_1^{-5/3}$  for  $R_\lambda = 1201$  DNS should be constant, but small negative slope  $\sim .1$  suggests that a more appropriate spectrum for the inertial range might be  $\sim k^{-\frac{5}{3}-0.1}$ .

This plot also shows the *bottleneck effect*, which is represented by the pronounced peak that is formed for wave numbers just larger than those in the inertial range. One explanation for this phenomenon is that in this range there is insufficient small-scale vortices to efficiently dissipate energy so that it accumulates to form a bump. This effect vanishes for high Re.

One explanation for the departure of small-scale turbulence from the -5/3 law is the fact that  $\epsilon$  is highly intermittent in space and time.

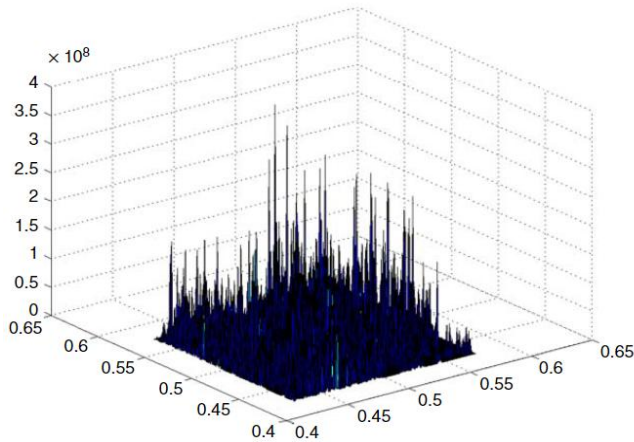


Figure 4.9 Dissipation rate on a plane showing intermittency within a region of isotropic turbulence computed in a vortex filament simulation of flow in a periodic box.

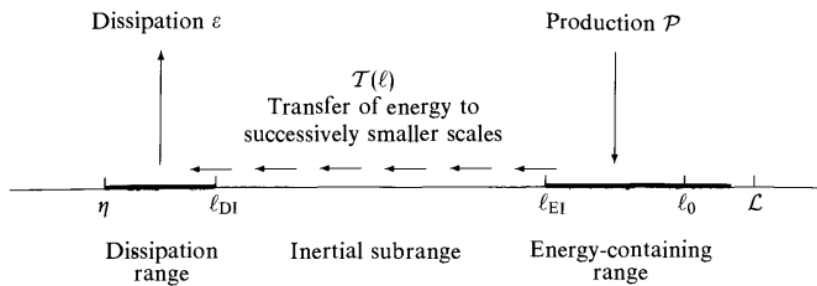
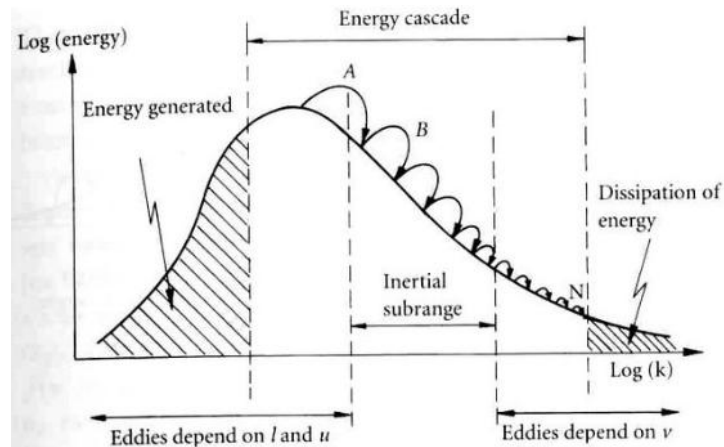


Fig. 6.2. A schematic diagram of the energy cascade at very high Reynolds number.



Clearly Kolmogorov -5/3 spectrum fully supports important turbulence concepts of Richardson cascade, Kolmogorov hypotheses, theory of isotropic turbulence and dimensional analysis; albeit with issues of backscatter suggesting energy transfer is a two-way equilibrium process including intermittency of dissipation.

## Taylor Frozen Turbulence Hypothesis

For small  $\Delta t$ , assume turbulence frozen as it convects past probe at  $x$  such that

Changes in measured  $U_i(t) \propto$  changes  $U_i(x)$ , i.e.,

$$\frac{dU_i}{dx} = -\frac{1}{U_c} \frac{dU_i}{dt}$$

Where  $U_c$  = convection velocity of frozen turbulence. Requires assumption  $\underline{a} = 0$  at  $x$  (i.e., sum of the pressure and viscous forces = 0)

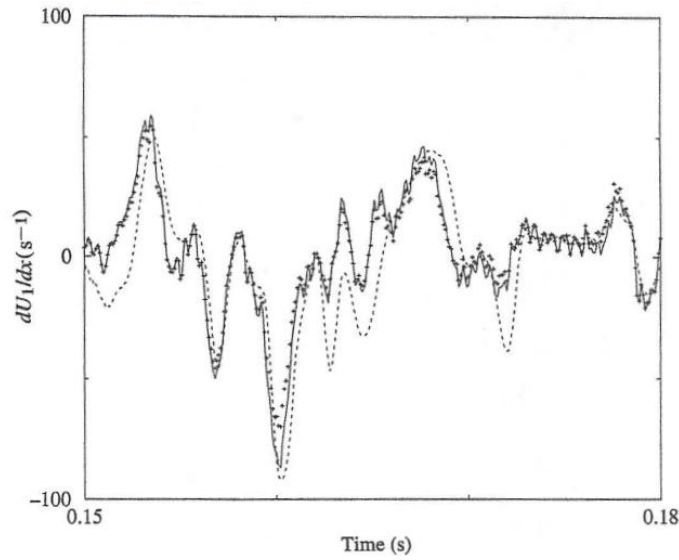
$$\frac{\partial U_i}{\partial t} + U_1 \frac{\partial U_i}{\partial x} + \cancel{U_2 \frac{\partial U_i}{\partial y}} + \cancel{U_3 \frac{\partial U_i}{\partial z}} = 0$$

That is, for the last 2 terms = 0 [i.e., 1-axis is aligned with the direction of the mean flow  $U_i = (U_1, 0, 0)$ ]

$$\frac{dU_i}{dx} = -\frac{1}{U_c} \frac{dU_i}{dt}$$

$$U_c = U_1$$

Must be far from solid boundaries such that viscous forces and turbulence intensities are not too large. Under such conditions, Taylors hypothesis does lead, on average, to good approximations of the streamwise derivatives of the velocity components.



Continuity:

$$\frac{\partial U_1}{\partial x} = -\left(\frac{\partial U_2}{\partial y} + \frac{\partial U_3}{\partial z}\right)$$

Fig. 3.5 Comparison of time-series signals determined from Taylor's hypothesis [Eqs. (3.30) — and (3.32) + + +] and from the continuity equation (· · ·) using mixing-layer data from a 12-sensor probe. (From [31].)

Reasonable agreement channel flow above buffer layer. Used to transform 1D  $f$  spectra to streamwise  $k$  spectra:

$$k_x \approx \frac{2\pi f}{U_1}$$

# Taylor's Frozen Turbulence Hypothesis

x-component WS neglected ✓

$$v_i = (0, 0, 0)$$

$$\frac{\partial \tilde{u}_1}{\partial t} + \tilde{u}_1' \frac{\partial \tilde{u}_1}{\partial x_1} + \tilde{u}_2' \frac{\partial \tilde{u}_1}{\partial x_2} + \tilde{u}_3' \frac{\partial \tilde{u}_1}{\partial x_3} = -\frac{1}{\rho} \frac{\partial \tilde{p}}{\partial x_1}$$

$$\tilde{u}_1 = u_1 + u_1'$$

$$\tilde{u}_2 = u_2 \quad \tilde{u}_3 = u_3$$

$$\tilde{p} = p + p'$$

$$\frac{\partial \tilde{u}_1}{\partial t} + \frac{\partial u_1'}{\partial t} + (u_1 + u_1') \frac{\partial (u_1 + u_1')}{\partial x_1} +$$

$$u_2' \frac{\partial (u_1 + u_1')}{\partial x_2} + u_3' \frac{\partial (u_1 + u_1')}{\partial x_3} = -\frac{1}{\rho} \frac{\partial (p + p')}{\partial x_1}$$

$$\frac{\partial u_1'}{\partial t} + u_1' \frac{\partial u_1'}{\partial x_1} = -\frac{1}{\rho} \frac{\partial p'}{\partial x_1} - u_1' \frac{\partial u_1'}{\partial x_1} - u_2' \frac{\partial u_1'}{\partial x_2} - u_3' \frac{\partial u_1'}{\partial x_3} - \frac{1}{\rho} \frac{\partial p'}{\partial x_1}$$

$$\frac{1}{\rho} \frac{\partial u_1'}{\partial t} + \frac{\partial u_1'}{\partial x_1} = \underbrace{-\frac{u_1'}{u_1} \frac{\partial u_1'}{\partial x_1} - \frac{u_2'}{u_1} \frac{\partial u_1'}{\partial x_2} - \frac{u_3'}{u_1} \frac{\partial u_1'}{\partial x_3}}_a - \frac{1}{\rho} \left[ \frac{\partial p'}{\partial x_1} + \frac{\partial p'}{\partial x_1} + \frac{\partial p'}{\partial x_1} + \frac{\partial p'}{\partial x_1} \right]$$

mean momentum equation:  $\frac{\partial \bar{u}_1}{\partial t} + \bar{u}_1' \frac{\partial \bar{u}_1}{\partial x_1} = -\frac{1}{\rho} \frac{\partial \bar{p}}{\partial x_1} - \frac{\partial \bar{p}'}{\partial x_1}$

$$\frac{1}{\rho} \frac{\partial u_1'}{\partial t} + \frac{\partial u_1'}{\partial x_1} = a - \frac{1}{\rho} \left[ -\frac{\partial \bar{p}'}{\partial x_1} + \frac{\partial p'}{\partial x_1} \right]$$

Assume statistically homogeneous  $\frac{\partial \bar{u}_1}{\partial x_i} = 0$

$$u_1' \approx \rho u_1'^2$$

$$RHS = -\frac{u_1'}{u_1} \frac{\partial u_1'}{\partial x_1} - \frac{u_2'}{u_1} \frac{\partial u_1'}{\partial x_2} - \frac{u_3'}{u_1} \frac{\partial u_1'}{\partial x_3} - \frac{1}{\rho} \left[ -\frac{\partial \bar{p}'}{\partial x_1} + \frac{\partial p'}{\partial x_1} \right]$$

$$= -\frac{u_1'}{u_1} \frac{\partial u_1'}{\partial x_1} - \frac{1}{\rho} \left[ \frac{\partial \bar{p}'}{\partial x_1} + \frac{\partial p'}{\partial x_1} \right]$$

∴ for  $\frac{u_1'}{u_1} \ll 1$  LHS = 0

That is:  $\frac{\partial u_1'}{\partial t} + \bar{u}_1' \frac{\partial u_1'}{\partial x_1} = 0$

Also see Pope pp 225-224

# The spectrum of turbulence

BY G. I. TAYLOR, F.R.S.

(Received 1 December 1937)

When a prism is set up in the path of a beam of white light it analyses the time variation of electric intensity at a point into its harmonic components and separates them into a spectrum. Since the velocity of light for all wave-lengths is the same, the time variation analysis is exactly equivalent to a harmonic analysis of the space variation of electric intensity along the beam. In a recent paper Mr Simmons (Simmons and Salter 1938) has shown how the time variation in velocity at a field point in a turbulent air stream can be analysed into a spectrum. In the present paper it is proposed to discuss the connexion between the spectrum of turbulence, measured at a fixed point, and the correlation between *simultaneous* values of velocity measured at two points.

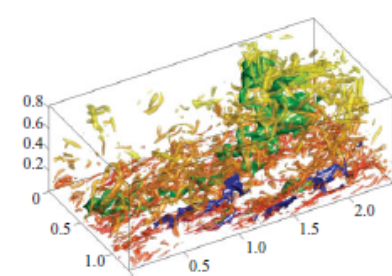
Taylor, G. I. 1938 The spectrum of turbulence. Proc. R. Soc. Lond. **164** (919), 476–490.

*Journal of Fluid Mechanics* **FF** Focus on fluids

## Revisiting Taylor's hypothesis

P. MOIN

Center for Turbulence Research, Stanford University,  
Stanford, CA 94305, USA



---

Taylor's hypothesis, relating temporal to spatial fluctuations in turbulent flows is investigated using powerful numerical computations by del Álamo & Jiménez (*J. Fluid Mech.*, 2009, this issue, vol. 640, pp. 5–26). Their results cast doubt on recent interpretations of bimodal spectra in relation to very large-scale turbulent structures in experimental measurements in turbulent shear flows.

---

## Revisiting Taylor's hypothesis in homogeneous turbulent shear flow

Frank G. Jacobitz <sup>1,\*</sup> and Kai Schneider <sup>2,†</sup>

<sup>1</sup>*Mechanical Engineering Department, Shiley-Marcos School of Engineering, University of San Diego,  
5998 Alcalá Park, San Diego, California 92110, USA*

<sup>2</sup>*Aix-Marseille Université, CNRS, Institut de Mathématiques de Marseille,  
3 place Victor Hugo, 13331 Marseille cedex 3, France*



(Received 28 September 2023; accepted 14 March 2024; published 3 April 2024)

Taylor's hypothesis of frozen flow is revisited in homogeneous turbulent shear flow by examining the cancellation properties of Eulerian and convective accelerations at different flow scales. Using results of direct numerical simulations, vector-valued flow quantities, including the Lagrangian, Eulerian, and convective accelerations, are decomposed into an orthogonal wavelet series and their alignment properties are quantified through the introduction of scale-dependent geometrical statistics. Joint-probability density functions of the Eulerian and convective accelerations show antialignment at small scales of the turbulent motion, but this observation does not hold at large scales. Similarly, the angles of the scale-wise contributions of the Eulerian and convective accelerations were found to prefer an antiparallel orientation at small scales. Such antialignment, however, is not observed at the largest scales of the turbulent motion. The results suggest that Taylor's hypothesis holds at small scales of homogeneous turbulent shear flow, but not for large-scale motion. The Corrsin scale is proposed as a measure for the applicability of Taylor's hypothesis in such flows.

## Appendix A

### A.1

$$E_{11}(\kappa_1) = C_1 A \kappa_1^{-p} \quad (1A)$$

$$E(\kappa) = \frac{1}{2} \kappa^3 \frac{d}{d\kappa} \left( \frac{1}{\kappa} \frac{dE_{11}(\kappa)}{d\kappa} \right) \quad (2A)$$

Substitute (1A) into (2A)

$$E(\kappa) = \frac{1}{2} \kappa^3 \frac{d}{d\kappa} \left( \frac{1}{\kappa} \frac{d(C_1 A \kappa^{-p})}{d\kappa} \right)$$

$$E(\kappa) = \frac{1}{2} \kappa^3 \frac{d}{d\kappa} \left( -\frac{1}{\kappa} C_1 A p \kappa^{-p-1} \right)$$

$$E(\kappa) = \frac{1}{2} \kappa^3 \frac{d}{d\kappa} (-C_1 A p \kappa^{-p-2})$$

$$E(\kappa) = \frac{1}{2} \kappa^3 (p+2) p C_1 A \kappa^{-p-3}$$

$$E(\kappa) = \underbrace{\frac{1}{2} (p+2) p C_1 A}_{C} \kappa^{-p}$$

$$C = \frac{1}{2} (p+2) p C_1$$

$$E(\kappa) = C A \kappa^{-p}$$

## A.2

$$E_{22}(\kappa_1) = E_{33}(\kappa_1) = \frac{1}{2} \left( E_{11}(\kappa_1) - \kappa_1 \frac{dE_{11}(\kappa_1)}{d\kappa_1} \right) \quad (3A)$$

Substituting Eq. (1A) into (3A) ( $\kappa = \kappa_1$ )

$$E_{22}(\kappa) = \frac{1}{2} (C_1 A \kappa^{-p} + \kappa C_1 A p \kappa^{-p-1})$$

$$E_{22}(\kappa) = \frac{1}{2} (C_1 A \kappa^{-p} + C_1 A p \kappa^{-p})$$

$$E_{22}(\kappa) = \underbrace{\frac{1}{2} C_1 (1 + p)}_{C_1'} A \kappa^{-p}$$

$$E_{22}(\kappa) = C_1' A \kappa^{-p}$$

$$C_1' = \frac{1}{2} (1 + p) C_1$$